JOURNAL OF GEOPHYSICAL RESEARCH, VOL. 111, A07101, doi:10.1029/2005JA011533, 2006

A three-dimensional MHD solar wind model with pickup protons

A. V. Usmanov[1,2] and M. L. Goldstein[3]

Received 30 November 2005; revised 22 February 2006; accepted 14 March 2006; published 7 July 2006.

[1] We have developed a three-dimensional (3-D) steady-state MHD model of the solar corona and solar wind that covers the region from the coronal base to 100 AU and that accounts for the effects of pickup protons in the distant heliosphere. The model expands the two-region model of Usmanov and Goldstein (2003) to include a region III that extends from 1–100 AU and incorporates a population of interstellar neutral hydrogen and its interaction with solar wind protons. Following the approach of Isenberg (1986) and Whang (1998), we consider the solar wind outside 1 AU as a combination of three comoving species, solar wind protons, electrons, and pickup protons, and solve the 3-D steady-state MHD equations with source terms due to photoionization and charge exchange. Separate energy equations are included for solar wind and pickup protons. We show that the pickup protons cause a deceleration of the solar wind and an increase in average plasma temperature with heliocentric distance beyond ~10 AU. We compute the global structure of the solar wind from the coronal base to 100 AU and compare our results with Voyager 1 and 2 observations.

Citation: Usmanov, A. V., and M. L. Goldstein (2006), A three-dimensional MHD solar wind model with pickup protons, *J. Geophys. Res.*, *111*, A07101, doi:10.1029/2005JA011533.

1. Introduction

[2] Owing to the Sun's movement through the local interstellar medium (LISM), interstellar neutral hydrogen enters the heliosphere at a speed of ~26 km s^{-1}. Inside the heliosphere, interstellar hydrogen atoms become ionized as a result of charge exchange with solar wind protons and photoionization by solar radiation. These two processes produce protons that are magnetized, get picked up by the interplanetary magnetic field, and become incorporated into the solar wind [e.g., *Blum and Fahr*, 1970; *Semar*, 1970; *Holzer*, 1972; *Isenberg*, 1986]. These pickup protons, however, form a distinct population in the solar wind because of their large thermal speed ($\approx V_{SW}$). The thermal pressure of the pickup protons in the distant heliosphere is much larger than the pressure of solar wind protons and electrons and is at least comparable to the magnetic pressure [*Burlaga et al.*, 1994, 1996]. As a result, the distant heliosphere is affected strongly by pickup protons. The energy and momentum redistribution between the pickup and solar wind protons causes a deceleration of the solar wind [*Semar*, 1970; *Holzer*, 1972; *Richardson et al.*, 1995] and an increase of average plasma temperature with heliocentric distance [*Fahr*, 1973; *Holzer and Leer*, 1973].

[3] There is an extensive literature describing simulations that deal with the interaction of the heliosphere with the LISM (see, e.g., review by *Zank* [1999]), but only a few deal with solar wind models that concentrate on the physical properties of the distant solar wind plasma as determined by the effects of pickup protons. Such models are mostly one-dimensional [*Semar*, 1970; *Holzer*, 1972; *Isenberg*, 1986; *Whang*, 1998; *Wang et al.*, 2000; *Wang and Richardson*, 2001; *Whang et al.*, 2003]. Meanwhile, existing two- and three-dimensional formulations [e.g., *Baranov and Malama*, 1993; *Pauls et al.*, 1995; *Zank et al.*, 1996; *Pauls and Zank*, 1996; *Linde et al.*, 1998; *Opher et al.*, 2003] emphasize modeling the interaction of the solar wind with the LISM and, consequently, use simple formulations of the solar wind sufficient to specify inner boundary conditions at ~1–30 AU.

[4] The purpose of present work is to develop a three-dimensional MHD model of steady solar wind that incorporates the effects of pickup protons. Following *Isenberg* [1986] and *Whang* [1998], we consider the solar wind as a combination of solar wind protons, electrons, and pickup protons and assume that all three species are moving with the same velocity **v**. The solar wind protons and interstellar neutrals are coupled by photoionization and charge exchange. The solar wind protons and pickup protons are described with separate energy equations. As initial condition for integrating the MHD equations from 1 AU to 100 AU we use the 1 AU output from the tilted-dipole model of *Usmanov and Goldstein* [2003] which is appropriate for solar minimum conditions. That model divides the simulation domain into two-regions: Region I from 1 to 20 $R_\odot$ ($R_\odot$ is the solar radius) where a steady-state solution

[1]Bartol Research Institute, University of Delaware, Newark, Delaware, USA.
[2]Also at NASA Goddard Space Flight Center, Code 612.2, Greenbelt, Maryland, USA.
[3]NASA Goddard Space Flight Center, Code 612.2, Greenbelt, Maryland, USA.

0148-0227/06/2005JA011533$09.00

is obtained using the time-relaxation approach, and an outer region II (20 $R_\odot$–1 AU) where the solution is constructed by integrating the governing MHD equations along radius. In the present work, we extend that model into the outer heliosphere by including a region III (1–100 AU) where we account for the effects of pickup protons. We then compare our results with Voyager 1 and 2 observations.

[5] The plan of the paper is as follows: In section 2 we describe the governing equations and discuss in detail the initial and boundary conditions used. The results of simulation are discussed in section 3 and section 4 contains a detailed comparison of the model calculations with Voyagers 1 and 2. A summary in section 5 concludes the paper.

2. Model Formulation

[6] The steady-state MHD equations for the solar wind including pickup protons [*Whang*, 1998] can be written in conservation form in the frame of reference corotating with the Sun as

$$\nabla \cdot (N_S \mathbf{v}) = -q_{ex}, \tag{1}$$

$$\nabla \cdot \left[\rho \mathbf{v}\mathbf{v} + \left(P + \frac{B^2}{8\pi}\right)\mathbf{I} - \frac{\mathbf{B}\mathbf{B}}{4\pi}\right] + \rho\left[\frac{GM_\odot}{r^2}\hat{r} + 2\boldsymbol{\Omega} \times \mathbf{v} + \boldsymbol{\Omega} \times (\boldsymbol{\Omega} \times \mathbf{r})\right] = -m_p\left(q_{ex}\mathbf{u} + q_{ph}\mathbf{w}\right), \tag{2}$$

$$\nabla \times (\mathbf{v} \times \mathbf{B}) = 0, \tag{3}$$

$$\nabla \cdot \left\{\left[\frac{\rho(v^2 - w^2)}{2} + \frac{2\gamma P_S}{\gamma - 1} + \frac{5}{2}P_I\right]\mathbf{v} + \frac{\mathbf{B}}{4\pi} \times (\mathbf{v} \times \mathbf{B})\right\} = -\rho u_r \frac{GM_\odot}{r^2} - q_{ex} m_p \left[\frac{u^2}{2} - (\mathbf{w} \cdot \mathbf{u}) + \frac{2\gamma P_S}{(\gamma - 1)\rho_S}\right], \tag{4}$$

$$\nabla \cdot (N_I \mathbf{v}) = q_{ex} + q_{ph}, \tag{5}$$

$$\nabla \cdot \left(\mathbf{v} P_I^{3/5}\right) = \left(q_{ex} + q_{ph}\right)\frac{m_p u^2}{5P_I^{2/5}}, \tag{6}$$

where the dependent variables are the velocity in the corotating frame **v**, the magnetic field **B**, the number density N_S and thermal pressure $P_S = N_S k_B T_S$ of solar wind protons, the number density N_I and thermal pressure $P_I = N_I k_B T_I$ of pickup protons. Other notations are the velocity in the inertial frame $\mathbf{u} = \mathbf{v} + \mathbf{w}$, where $\mathbf{w} = \boldsymbol{\Omega} \times \mathbf{r}$ and $w = |\mathbf{w}|$, the siderial rotation rate of the Sun $\boldsymbol{\Omega}$, the total pressure $P = P_S + P_E + P_I$, the density $\rho = m_p(N_S + N_I)$, the heliocentric distance r, the temperatures of the solar wind protons, T_S, and of the pickup protons, T_I, the proton mass m_p, the gravitational constant G, the solar mass $M_\odot$, the unit vector in the radial direction $\hat{r}$. It is assumed that $P_E = P_S$, where P_E is the electron thermal pressure. The polytropic index γ for solar wind protons is taken to be 1.46 as inferred by *Totten et al.* [1995] using proton data from the Helios 1 spacecraft. This nonadiabatic value of γ is assumed to account implicitly for thermal conduction and turbulent heating processes in the solar wind [*Verma et al.*, 1995].

[7] The production rate of interstellar pickup protons (per unit volume per unit time) by charge exchange with solar wind protons and the production rate from photoionization are, respectively,

$$q_{ex} = \sigma N_S N_H u, \qquad q_{ph} = \nu_0 \left(\frac{r_0^2}{r^2}\right) N_H,$$

where N_H is the number density of the neutral interstellar hydrogen, $\sigma = 2 \times 10^{-15}$ cm^2 is the mean charge exchange cross section of hydrogen atoms, and $\nu_0 = 0.9 \times 10^{-7}$ s^{-1} is the rate of photoionization per hydrogen atom at the heliocentric distance $r_0 = 1$ AU [see *Whang* 1998].

[8] In corotating coordinates, in the absence of a steady electric field, the vectors of velocity and magnetic field are parallel [*Weber and Davis*, 1967; *Pizzo*, 1982]. The magnetic field components B_θ and B_ϕ can be then obtained from the relations: $B_\theta = v_\theta B_r/u_r$ and $B_\phi = v_\phi B_r/u_r$. The scalar $\nabla \cdot \mathbf{B} = 0$ equation can be then integrated instead of the vector induction equation (3) [*Pizzo*, 1982]. Assuming spherical coordinates (r, θ, ϕ) and using the following nondimensional parameters: the Rossby number $R_o = \Omega\tilde{L}/\tilde{u}$, the Euler number $E_u = \tilde{P}/\tilde{\rho}\,\tilde{u}^2$, the Froude number $F_r = \tilde{u}^2\tilde{L}/GM_\odot$, and the Alfvén Mach number $M_A = \tilde{u}(4\pi\tilde{\rho})^{1/2}/\tilde{B}$, where $\tilde{L}$, $\tilde{T}$, $\tilde{\rho}$, $\tilde{u}$, $\tilde{B}$, and $\tilde{P}$ are the units of length, time, density, velocity, magnetic field, and pressure, respectively, (1)–(6) can be rewritten in vector form

$$\frac{\partial \mathbf{W}}{\partial r} = \frac{\partial \mathbf{F}}{\partial \theta} + \frac{\partial \mathbf{G}}{\partial \phi} + \mathbf{S}, \tag{7}$$

where **W**, **F**, **G**, and **S** are the column vectors of 8 elements given by

$$\mathbf{W} = \begin{pmatrix} r^2\rho_S u_r \\ r^2\rho\left(u_r^2 + \frac{PE_u}{\rho} + \frac{V_{A\theta}^2 + V_{A\phi}^2 - V_{Ar}^2}{2}\right) \\ r^3\rho(u_r u_\theta - V_{Ar}V_{A\theta}) \\ r^3\rho\left(u_r u_\phi - V_{Ar}V_{A\phi}\right) \\ r^2 B_r \\ r^2\rho\left\{u_r\left[\frac{u^2}{2} + \frac{2\gamma P_S E_u}{(\gamma-1)\rho} + \frac{5P_I E_u}{2\rho}\right] - V_{Ar}\left(w_\theta V_{A\theta} + w_\phi V_{A\phi}\right)\right\} \\ r^2\rho_I u_r \\ r^2 u_r P_I^{3/5} \end{pmatrix}, \tag{8}$$

$$\mathbf{F} = -\begin{pmatrix} r\rho_S v_\theta \\ r\rho(u_r v_\theta - V_{Ar}V_{A\theta}) \\ r^2\rho\left(u_\theta v_\theta + \frac{PE_u}{\rho} + \frac{V_{Ar}^2 + V_{A\phi}^2 - V_{A\theta}^2}{2}\right) \\ r^2\rho\left(v_\theta u_\phi - V_{A\theta}V_{A\phi}\right) \\ rB_\theta \\ r\rho\left\{v_\theta\left[\frac{u^2}{2} + \frac{2\gamma P_S E_u}{(\gamma-1)\rho} + \frac{5P_I E_u}{2\rho}\right] - w_\phi V_{A\theta}V_{A\phi} + w_\theta\left(\frac{V_{Ar}^2 + V_{A\phi}^2 - V_{A\theta}^2}{2} + \frac{PE_u}{\rho}\right)\right\} \\ r\rho_I v_\theta \\ r v_\theta P_I^{3/5} \end{pmatrix}, \tag{9}$$

$$\mathbf{G} = -\frac{1}{\sin\theta}\begin{pmatrix} r\rho_S v_\phi \\ r\rho\left(u_r v_\phi - V_{Ar}V_{A\phi}\right) \\ r^2\rho\left(u_\theta v_\phi - V_{A\theta}V_{A\phi}\right) \\ r^2\rho\left(u_\phi v_\phi + \dfrac{PE_u}{\rho} + \dfrac{V_{Ar}^2 + V_{A\theta}^2 - V_{A\phi}^2}{2}\right) \\ rB_\phi \\ r\rho\left\{v_\phi\left[\dfrac{u^2}{2} + \dfrac{2\gamma P_S E_u}{(\gamma-1)\rho} + \dfrac{5P_I E_u}{2\rho}\right]\right. \\ \quad + w_\phi\left(\dfrac{V_{Ar}^2 + V_{A\theta}^2 - V_{A\phi}^2}{2}\right. \\ \quad \left.\left. + \dfrac{PE_u}{\rho}\right) - w_\theta V_{A\theta}V_{A\phi}\right\} \\ r\rho_I v_\phi \\ r v_\phi P_I^{3/5} \end{pmatrix}, \quad (10)$$

$$\mathbf{S} = -\begin{pmatrix} r\rho_S v_\theta \cot\theta + r^2\hat{q}_{ex} \\ r\rho\left[\cot\theta(u_r v_\theta - V_{Ar}V_{A\theta}) - u_\theta^2 - u_\phi^2\right. \\ \quad \left. + \dfrac{1}{F_r r} - \dfrac{2PE_u}{\rho} - V_{Ar}^2\right] + r^2\hat{q}_{ex}u_r \\ r^2\rho\left[\cot\theta\left(u_\theta v_\theta - u_\phi^2 - V_{A\theta}^2 + V_{A\phi}^2\right)\right. \\ \quad \left. + \dfrac{\overline{R_o r\sin\phi u_\phi}}{\sin\theta}\right] + r^3\hat{q}_{ex}u_\theta \\ r^2\rho\left[2\cot\theta\left(u_\theta u_\phi - V_{A\theta}V_{A\phi}\right)\right. \\ \quad \left. - w_\theta u_\phi\cot\theta - \dfrac{\overline{R_o r\sin\phi u_\theta}}{\sin\theta}\right] \\ \quad + r^3\hat{q}_{ex}u_\phi \\ r\cos\theta B_\theta \\ \dfrac{\rho u_r}{F_r} + r\rho\cos\theta\left\{v_\theta\left[\dfrac{u^2}{2} + \dfrac{2\gamma P_S E_u}{(\gamma-1)\rho}\right.\right. \\ \quad \left. + \dfrac{5P_I E_u}{2\rho}\right] - w_\phi V_{A\theta}V_{A\phi} \\ \quad \left. + w_\theta\left(\dfrac{V_{Ar}^2 + V_{A\phi}^2 - V_{A\theta}^2}{2} + \dfrac{PE_u}{\rho}\right)\right\} \\ \quad + r^2\hat{q}_{ex}\left[\dfrac{u^2}{2} + \dfrac{2\gamma P_S E_u}{(\gamma-1)\rho_S}\right] \\ r\rho_I v_\theta\cot\theta - r^2\left(\hat{q}_{ex} + \hat{q}_{ph}\right) \\ r\cot\theta v_\theta P_I^{3/5} - \dfrac{r^2u^2\left(\hat{q}_{ex} + \hat{q}_{ph}\right)}{5P_I^{2/5}E_u} \end{pmatrix}, \quad (11)$$

where $v_\theta = u_\theta - w_\theta$, $v_\phi = u_\phi - w_\phi$, $V_{Ar,\theta,\phi} = B_{r,\theta,\phi}/M_A\sqrt{\rho}$, $\hat{q}_{ex} = \rho_S\rho_H u K_1$, $\hat{q}_{ph} = \rho_H r_0^2 K_2/r^2$, $K_1 = \sigma\tilde{\rho}\tilde{L}/m_p$, $K_2 = \nu_0\tilde{L}/\tilde{u}$, and $u^2 = u_r^2 + u_\theta^2 + u_\phi^2$. [The two terms in **S** with upper bars are discussed below.]

[9] To circumvent the geometrical singularity on the pole and the concentration of grid cells around the polar axis in spherical coordinates, equation (7) solved on a composite grid composed of a main spherical grid that extends in latitude from $-67°$ to $+67°$ with the spacing $\Delta\theta = \Delta\phi = 3°$, and two "polar patches" covering the polar regions which are fragments of a spherical grid with its polar axis rotated by 90° with respect to the main grid [*Usmanov*, 1996]. The main and polar grids are overlapped in such a manner that the boundary values of each grid are computed by interpolation from inner points of the overlapping grids. The governing MHD equations are the same for all grids except for the terms describing the solar rotation. For the main grid, $w_\theta = 0$ and $w_\phi = R_o\, r\,\sin\theta$, while for the polar grids, with their polar axis lying in the meridional plane $w_\theta = -R_o r\cos\phi$ and $w_\phi = R_o r\cos\theta\sin\phi$. In addition, two extra terms appear in the source terms of the meridional and azimuthal momentum equations for the polar grids; these terms are shown with upper bars in (11) and disappear for the main grid.

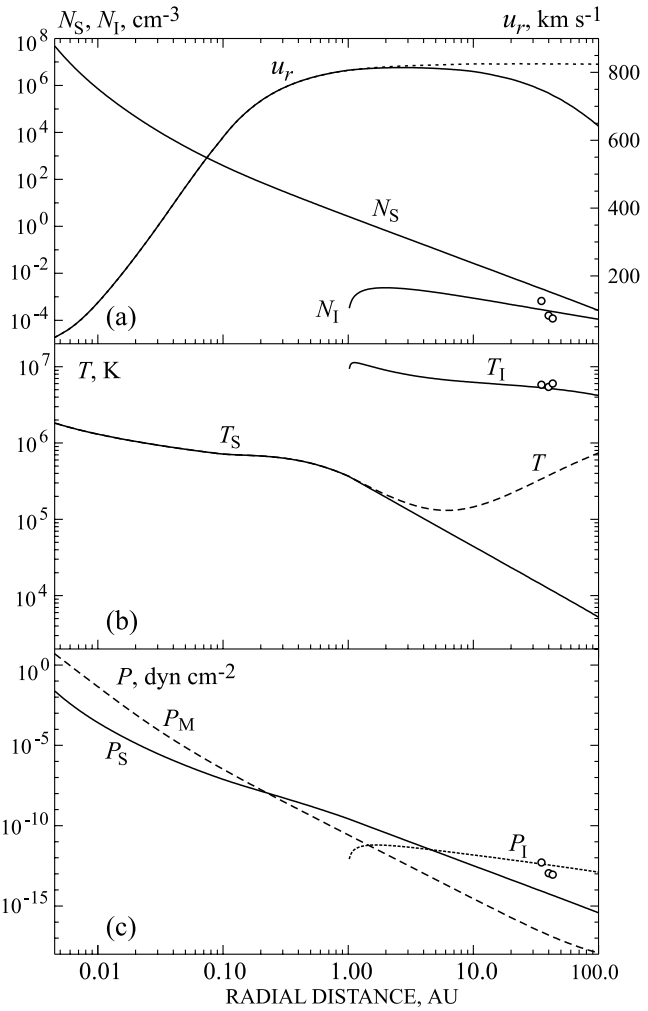

Figure 1. The variations versus heliocentric distance from 1 $R_\odot$ to 100 AU near the polar axis of (a) the radial velocity u_r, the solar wind proton density N_S and the pickup proton density N_I; the dashed line shows the solution without pickup protons; (b) the solar proton temperature T_S, the pickup proton temperature T_I, and the mean plasma temperature $T = (2N_S\,T_S + N_I\,T_I)/(2N_S + N_I)$; (c) the solar wind proton pressure P_S, the pickup proton pressure P_I, and the magnetic pressure P_M. The small circles present the values of N_I, T_I, and P_I inferred by *Burlaga et al.* [1994, 1996] from Voyager 2 observations of pressure-balanced structures near 35, 39–41, and 43 AU.

[10] A consequence of writing down the steady-state governing equation (7) in the corotating frame is that interstellar neutral hydrogen is assumed to be distributed uniformly throughout the heliosphere; otherwise, the hydrogen would constitute a time-dependent source term that would violate our steady-state assumption. Our prime interest is, however, the effects of pickup protons on solar

wind structure and we are not trying to model the heliospheric distribution of neutrals. Consequently, our use of a uniform distribution of neutral hydrogen appears to be acceptable. In the calculations below, we use $N_H = 0.1$ cm^{-3}. We should note here that the uniform distribution of neutral hydrogen is just a simplifying assumption (see, e.g., a discussion by *Pauls and Zank* [1997] on how the nonuniform neutrals affect the large-scale morphology of the solar wind) and we plan to relax this assumption in future.

[11] Equation (11) is hyperbolic with respect to the radial coordinate in the region where the flow is supersonic and super-Alfvénic [*Pizzo*, 1982] and thus can be integrated using the initial distribution of dependent parameters at 1 AU outward step-by-step along the radius up to any given heliocentric distance (100 AU in our case). To perform the integration, we use the MacCormack numerical method [*MacCormack*, 1971] combined with the artificial diffusion scheme suggested by [*Pizzo*, 1982]. The step along radius is defined by the Courant-Friedrichs-Lewy condition $\Delta r \leq \min(\Delta\theta/\max|\lambda_\theta|, \Delta\phi/\max|\lambda_\phi|)$, where

$$\lambda_\theta = \frac{-v_\theta u_r^3 \pm \left[\left(\alpha + u_r^4\right)\left(u_r^2 v_\theta^2 - \alpha\right)\right]^{1/2}}{r\alpha},$$

$$\lambda_\phi = \frac{-v_\phi u_r^3 \pm \left[\left(\alpha + u_r^4\right)\left(u_r^2 v_\phi^2 - \alpha\right)\right]^{1/2}}{r\sin\theta\alpha},$$

and

$$\alpha = V_{Ar}^2\left(v_\theta^2 + v_\phi^2\right) - \left(u_r^2 - V_{Ar}^2\right)\left(u_r^2 - c_S^2\right),$$

$$c_S^2 = (\gamma P_S + 5P_I/3)\frac{E_u}{\rho}.$$

To start integration of (7) out to 100 AU, we use the output at 1 AU from the model of *Usmanov and Goldstein* [2003] in which a steady coronal outflow in the tilted-dipole magnetic field (the dipole axis is inclined by $\sim$10° to the solar rotation axis) was simulated with a WKB Alfvén wave influx into open field regions. A bimodal structure of fast and slow wind was obtained that agreed with Ulysses observations during its first fast latitude scan in 1994–1995. The initial distributions of the radial velocity, density, and radial magnetic field at 1 AU are shown in Figure 5 of *Usmanov and Goldstein* [2003]. Other input parameters at 1 AU include the number density of pickup protons $N_{I0} = 1.5 \times 10^{-4}$ cm^{-3} and their temperature $T_{I0} = 6.35 \times 10^6$ K [after *Whang* 1998].

3. Simulation Results and Analysis

[12] Figure 1 shows radial variations of solar wind parameters in the region from the coronal base to 100 AU along a line near the polar axis ($\theta = 1.5°$). The velocity of the fast polar solar wind increases from $\sim$20 km s^{-1} at 1 $R_\odot$ to $\sim$800 km s^{-1} at 1 AU [see *Usmanov et al.*, 2000; *Usmanov and Goldstein*, 2003] and then decreases beyond 5 AU to $\sim$630 km s^{-1} at the outer boundary of 100 AU. The slowdown is clearly due to the interaction of solar wind plasma with neutral hydrogen as the solution neglecting the interstellar hydrogen (dashed curve) shows no deceleration. Figure 1a shows also the variations of N_S and N_I with heliocentric distance. N_S falls off faster than r^{-2} until the wind acceleration is mostly completed (by $\sim$30 $R_\odot$) and then throughout the heliosphere its decrease follows the r^{-2} law without obvious regard for the wind deceleration. The solution for N_S with no interstellar hydrogen is very close to that shown in Figure 1a (the deviation is 1% within 50 AU and $\sim$5% at 100 AU) and essentially overlaps with it due to logarithmic scale used. The small effect of neutral hydrogen on N_S is due to balance between the increase in N_S associated with a decrease in velocity and the decrease in N_S produced by an increase in N_I.

[13] At 1 AU the temperature of solar wind protons is $T_S \sim 3.5 \times 10^5$ K, which is about 30 times lower than the pickup proton temperature ($T_I \sim 10^7$ K). The ratio raises quickly with r as T_I is only slightly dependent of r and $T_S \approx r^{-2(\gamma-1)} \approx r^{-0.92}$. The mean temperature of the three plasma species $T \approx (2N_S T_S + N_I T_I)/(2N_S + N_I)$ (where the factor of 2 represents the contribution from electrons) reaches a minimum of 1.5×10^5 K at $\sim$7 AU and then increases to $\sim 7 \times 10^5$ K at 100 AU. The solar wind proton pressure P_S is shown in Figure 1c along with the pickup proton pressure P_I and the magnetic pressure P_M. P_M dominates in the near-Sun region out to $\sim$0.2 AU where P_S begins to dominate. However, outside 5 AU, the dominant pressure is P_I which becomes $\sim$100 times greater than P_S and $\sim 10^5$ times greater than P_M by 100 AU.

[14] Small circles in Figure 1 present the estimates of N_I, T_I, and P_I inferred by *Burlaga et al.* [1994] and *Burlaga et al.* [1996] from their analysis of pressure-balanced structures observed by Voyager 2 near 35, 39–41, and 43 AU. It is clear that the computed curves fit reasonably well with the pickup proton parameters determined from observations [cf. *Whang et al.*, 1996]. In general, the results shown in Figure 1 are similar to those in the one-dimensional study of *Whang* [1998]. The dominance of pickup proton pressure in the distant heliosphere leads to a slowdown and to an effective heating of the solar wind. Unlike *Whang* [1998], the computed magnetic pressure P_M is much smaller than P_S beyond 1 AU because close to the pole the azimuthal magnetic field is negligible and $P_M \approx B_r^2/8\pi \sim r^{-4}$, whereas near the equator $P_M \approx B_\phi^2/8\pi \sim r^{-2}$.

[15] Figure 2 shows contour maps of the computed flow parameters in the meridional plane $\phi = 0°$ with logarithmic scaling of the radial coordinate from 1 $R_\odot$ to 100 AU. (Note: After the computations are completed the output is mapped onto a single uniform spherical mesh for display purposes.) The radial velocity pattern is bimodal and comprises a slower wind band warping around the equator above the stagnation region (where the plasma velocity is virtually zero) and the fast wind, which is only slightly dependent on latitude, filling the rest of the heliosphere. Deceleration of the fast wind is discernible as a slight "limb" darkening beyond $\sim$10 AU. Corresponding patterns of solar proton density N_S, meridional velocities u_θ, solar proton temperature T_S, pickup proton density N_I, and pickup proton temperature T_I are shown in Figures 2b–2f. The meridional flows redistribute mass flux in latitude and

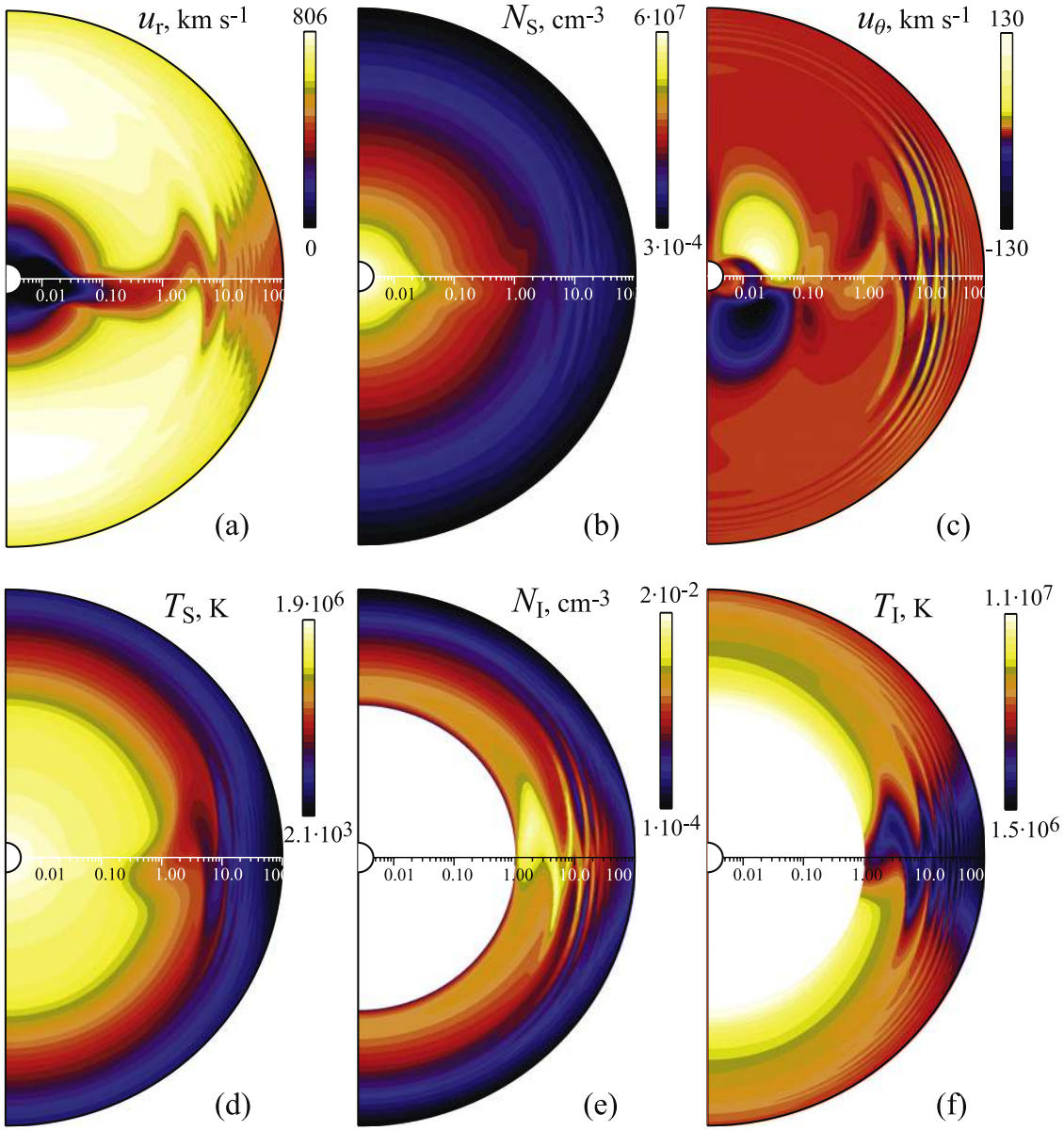

Figure 2. Contour plots in the meridional plane at $\phi = 0°$ of (a) the radial velocity, (b) number density of solar wind protons, (c) meridional velocity, (d) temperature of solar wind protons, (e) number density of pickup protons, and (f) pickup proton temperature. The radial coordinate extends from 1 $R_\odot$ to 100 AU and is scaled logarithmically.

create a belt of higher density near the equator (heliospheric plasma sheet). As the pickup proton effects are included in the model computations just outside 1 AU, the regions $r <$ 1 AU appear as white areas in Figures 2e–2f. In addition, we show in Figure 3 contour maps of B_r with the twisting heavy white line depicting the values $B_r = 0$, i.e., the heliospheric neutral sheet (embedded into the heliospheric current sheet) that separates regions of the solar wind where the magnetic field points toward or away from the Sun. In our simulation, the warp of the neutral sheet is slowly decreasing with distance beyond several AUs.

[16] Figure 4 shows latitudinal variations of the radial velocity, solar proton density, and also solar proton temperature in the meridional plane $\phi = 0$ for a number of heliocentric distances from 1 $R_\odot$–100 AU. The velocity varies only slightly with latitude except for a slower wind around the stagnation region and near the heliospheric plasma sheet. The transition between slow and fast wind becomes less sharp as heliocentric distance increases. The tilt of source dipolar magnetic field and subsequent fast-slow stream interactions produce a north-south asymmetry of the velocity profiles in which the velocity gradient is steeper in the northern hemisphere in this particular meridional plane. The slow wind is always more dense (Figure 4b) so that the mass flux is only slightly dependent of latitude. In the distant solar wind, the latitudinal variation of solar proton temperature T_S correlates in general with flow velocity, with the slow wind temperature being several

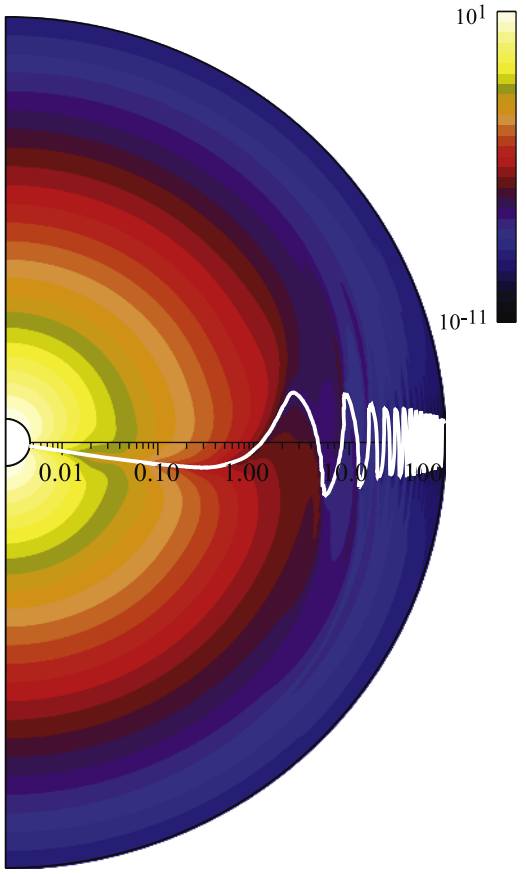

Figure 3. Contour plot in the meridional plane at $\phi = 0°$ of $|B_r|$ in Gauss. The heavy white line depicts the heliospheric neutral sheet.

times lower than the fast wind temperature at the same radial distance. [cf. *Phillips et al.*, 1995].

4. Comparison With Voyager 1 and 2

[17] *Usmanov et al.* [2000] and *Usmanov and Goldstein* [2003] compared the model output with Ulysses data during Ulysses' first fast latitude transition in 1994–1995 and demonstrated an overall agreement between the observed and simulated latitudinal profiles. As we have extended the model into the outer heliosphere, we can now compare directly our results with Voyager 1 and 2 measurements. Figure 5 shows model profiles computed along Voyager 1 and 2 trajectories against the observations from 13 September 1994 to 31 August 1995 when Voyager 1(2) was at heliocentric distances 57.0–60.5(43.9–46.7) AU and at heliolatitudes 32.6–32.8°(12.4–14.4°) north (south) of heliocentric equator. The computed profiles of solar proton density, radial velocity, and solar proton temperature versus Voyager 2 observations are shown in Figures 5a–5c. The computed magnetic field magnitudes are plotted versus Voyager 1 and 2 magnetic field observations in Figures 5d–5e. As can be seen, the model density compares reasonably well to the average Voyager 2 data. The model radial velocity is on average slightly higher (20–30 km s^{-1}) than that observed, but its simulated variations with the solar rotation period, while being smaller in magnitude, tend to be in phase with those in the observed velocity. The computed solar proton temperature T_S is ~2 times smaller, but again the simulated and observed variations with solar rotation appear to be well correlated.

[18] In present model, the energy balance of solar wind protons is governed by the polytropic index γ. We use $\gamma = 1.46$, as suggested by Helios data within 1 AU [*Totten et al.*, 1995]. This is different from the adiabatic value of 5/3 and thus implies an additional heating of solar wind protons. This heating can be attributed to thermal conduction, turbulent cascade, stream interactions, shock waves dissipation, etc. [see, e.g., *Verma et al.* 1995]. In our model, the pickup and solar wind protons are different species with different temperatures. It is possible that in reality some additional redistribution of pickup proton thermal energy

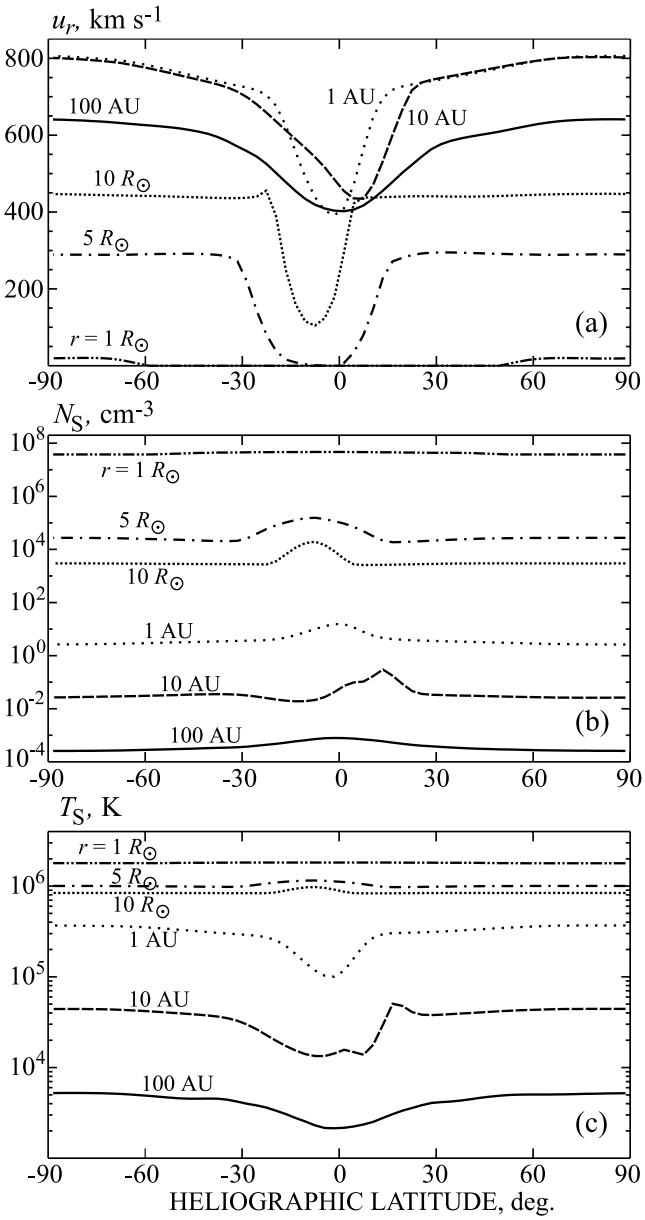

Figure 4. The radial velocity u_r, solar wind proton number density N_S, and temperature T_S versus heliographic latitude at the indicated radial distances in the meridional plane $\phi = 0°$.

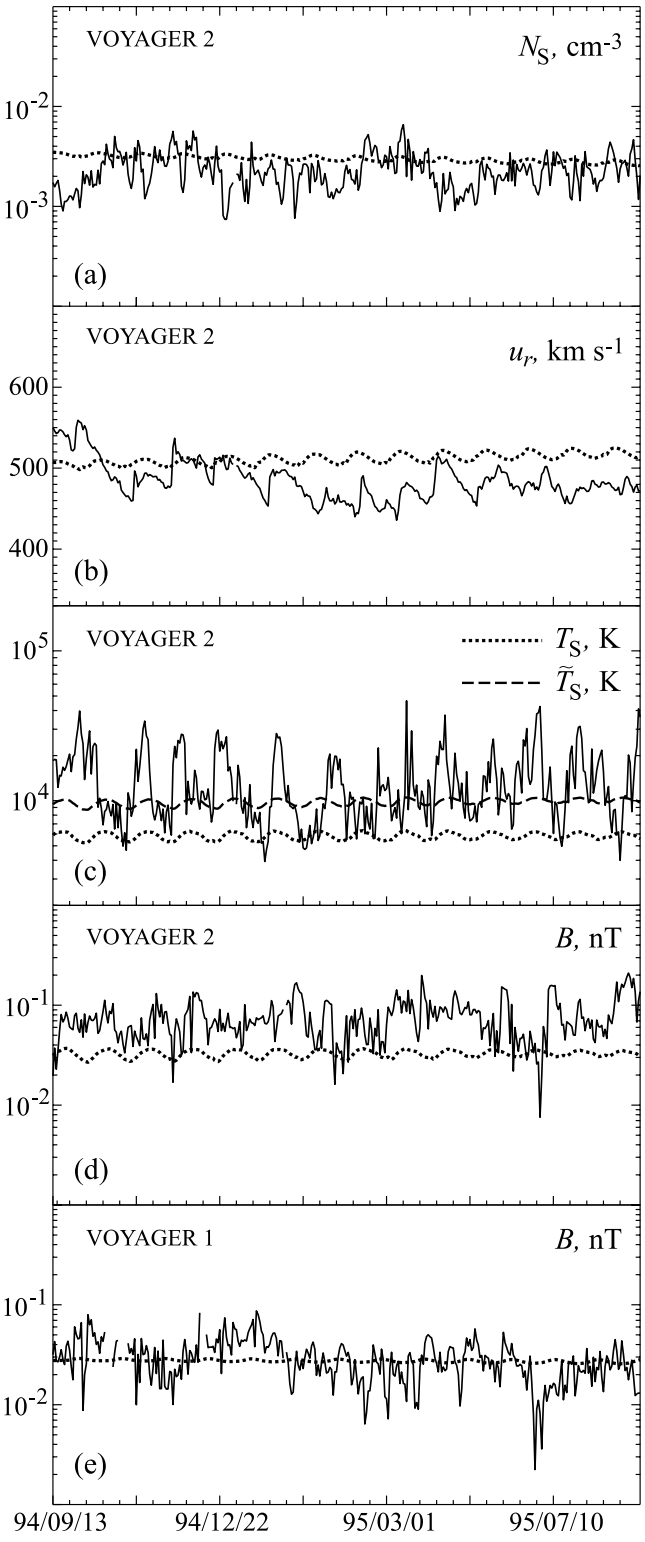

Figure 5. The model output (dotted lines) versus Voyager 1 and 2 measurements (solid lines) in 1994–1995 of proton density, speed, temperature and magnetic field magnitude.

takes place by which solar wind protons acquire a small fraction of the pickup proton energy. The dashed curve in Figure 5c represents the case of pickup protons contributing 1% of their energy to solar wind protons. This gives a better fit to the Voyager 2 observations. The two bottom panels of Figure 5 show the computed magnitude of magnetic field and that measured by Voyager 1 and 2 in 1994–1995. The model matches the average field magnitudes as observed with Voyager 1 while the Voyager 2 magnitudes are 2–3 times larger than those produced by the model.

[19] In Figure 6 we show radial variations of solar wind and magnetic field parameters computed along the trajectories of Voyager 1 and 2 from 1 to ~75 AU. Also shown are the heliographic latitudes of each spacecraft and solar activity variations from 1977 to 2004. Voyager 1 started its climbing into the northern heliosphere after its encounter with Saturn in November 1980 and it reached the latitude of 30°N in 1988. Since then its latitude has been slowly increasing (33.5°N in 1999). Voyager 2 stayed much longer near the helioequator and its excursion below the ecliptic plane began in 1989 following its encounter with Neptune at ~30 AU. It reached the latitude of 25.7°S in 2004. The deviations of both spacecraft from equatorial plane appear to be significant enough to study latitudinal dependencies in the data. In Figure 6 we show additional model profiles computed along Voyager pseudo-trajectories assumed to be the projections of real trajectories onto the helioequatorial plane. The model curves for the real and pseudo-trajectories differ considerably outside of 10 AU (30 AU) for Voyager 1 (2). The deviation is indicative of the latitudinal effect that is contained in the Voyager observations.

[20] During periods of low solar activity, the solar wind is slower and denser near the equatorial plane than at other latitudes (see Figure 4). Consequently, owing to emerging into faster wind both Voyagers observed generally lower densities and higher speeds than if they had remained in the equatorial plane. Magnetic field magnitude and proton plasma temperature are also increasing functions of latitude, and the solid and dashed model curves deviate significantly again. The most interesting aspect is that the combined effect of radial and latitude changes in Voyager 2 observations can cause the magnetic field and solar proton temperature to not decrease monotonically with distance in the outer heliosphere. The flattening of the radial temperature profile was first attributed to latitudinal gradients by *Gazis et al.* [1994] who compared the proton temperature observations from Pioneer 10, Pioneer 11, and Voyager 2, while Pioneer 11 was at 17°N and both Pioneer 10 and Voyager 2 were near the solar equator. This effect is especially important in view of the interpretation of proton temperature variations observed by Voyager 2 as an indication and measure of extensive heating of the expanding solar wind plasma due to a turbulent cascade, pickup proton heating, etc. [e.g., *Williams et al.*, 1995; *Verma et al.*, 1995; *Richardson and Smith*, 2003; *Isenberg et al.*, 2003; *Smith et al.*, 2004]. One should note that if in reality the slow-dense wind band was narrower compared to that produced by our simulation, then the latitudinal effect could be even stronger and the proton temperature along Voyager 2's orbit (solid curve in Figure 6) could even be increasing beyond 30 AU.

[21] We superposed the 27-day running average data of Voyager 1 and 2 in Figure 6 to show that the data is in general agreement with the model profiles. We should recall that the tilted-dipole model describes a bimodal solar wind structure that is characteristic of solar minimum and in general is not appropriate for other phases of solar cycle.

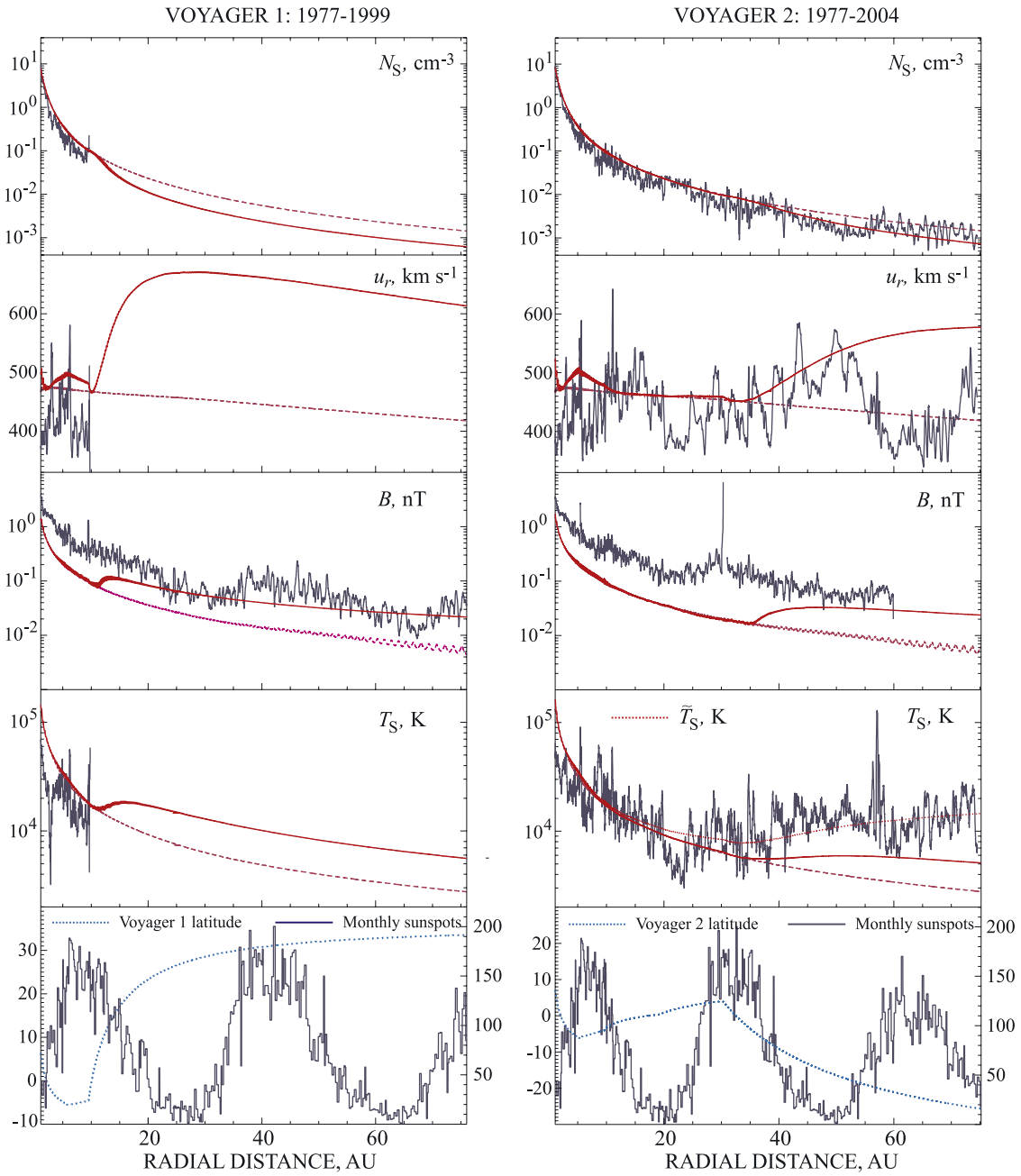

Figure 6. Radial variations of model parameters (red solid curves) computed along the trajectories of Voyager 1 (left) and Voyager 2 (right panels). The dark blue lines represent 27-day running averages of Voyager plasma and magnetic field data. The two bottom plots show the monthly sunspot numbers and heliographic latitudes of each spacecraft. The model parameters computed along pseudo-trajectories assuming that both spacecraft stay in the helioequatorial plane are shown with the dashed curves. Note that the model of tilted-dipole is appropriate only for periods of low solar activity.

While the densities measured by Voyager 2 do not appear strongly affected by changes in solar activity (shown in bottom panels), it is apparent that the observed speeds tend to anticorrelate with the sunspot numbers and the same is true to a lesser degree for the proton temperature. As a result, the measured densities are reproduced reasonably well for the entire period of Voyager observations. At the same time, the solar wind speeds observed by Voyager 2 are significantly lower than those computed during the period of high solar activity in 1998–2003 when the spacecraft moved from 55 to 70 AU. The magnetic field intensity shows a tendency to change in phase with solar activity, at least for Voyager 2 data. The model tends to fit the Voyager 1 data, but the Voyager 2 data lies above the model curve even beyond 40 AU. The radial temperature profile as observed by Voyager 2 clearly shows that the proton temperature does not generally decrease with distance beyond ~30–40 AU [cf. *Williams et al.*, 1995]. The apparent "inflexion" point is roughly coincident with the beginning of Voyager 2's descending under the equatorial

plane. Hence it appears plausible to at least partially ascribe the nondecreasing behavior of proton temperature beyond 30–40 AU to a latitudinal gradient. This effect, as estimated from our present simulation, is not sufficient to account for the higher temperatures observed outside 30–40 AU. However, if we assume again that solar wind protons additionally acquire a 1% fraction of the pickup proton energy than we arrive to a much better fit to the temperature observed by Voyager 2 (dotted curve).

5. Summary

[22] We have computed the global three-dimensional structure of the solar wind and interplanetary magnetic field from the base of solar corona to 100 AU under steady-state conditions and compared the simulated plasma and magnetic field parameters with Voyager 1 and 2 measurements. Our tilted-dipole model is built on the simulation study of *Usmanov and Goldstein* [2003] and is most appropriate for solar minimum conditions. The model assumes a uniform distribution of neutral hydrogen throughout the heliosphere and accounts for the processes of photoionization and charge exchange between solar wind protons and pickup protons. The simulation results are consistent with earlier studies in showing that the pickup protons cause a deceleration of the solar wind beyond 10 AU and an increase in average plasma temperature with heliocentric distance. We show that the model output is also in reasonable agreement with the estimates of pickup proton density, temperature, and thermal pressure derived by *Burlaga et al.* [1994] and *Burlaga et al.* [1996] from observations of pressure-balanced structures by Voyager 2 near 35, 39–41, and 43 AU.

[23] *Usmanov and Goldstein* [2003] demonstrated that present model is in agreement with Ulysses observations during its first fast latitude transit in 1994–1995. In the present work we show that the model is also roughly consistent with Voyager 1 and 2 observations during that period except that it predicts significantly lower values of magnetic field magnitude along the Voyager 2 trajectory than is observed. Also, to match the proton temperatures measured by Voyager 2 we made the ad hoc assumption that a small fraction (1%) of pickup proton energy is transferred to solar wind protons.

[24] The three-dimensional character of present model allowed us to estimate the latitudinal effect contained in the Voyager 2 data. Owing to latitudinal gradients which are relatively strong, at least around solar minimum, the descent of Voyager 2 to higher southern latitudes (as it is moving away from the Sun) causes a flattening of radial profiles of magnetic field intensity and proton temperature. Again, the model shows a good fit to the proton temperature measurements if the solar wind protons acquire 1% of thermal energy of pickup protons (in addition to the heating implicit in using a non-adiabatic polytropic index $\gamma = 1.46$).

[25] The proposed solar wind model can be useful in studies of the global heliospheric structure and the interaction of solar wind with the LISM. Work is in progress to relax the assumption of polytropic flow with $\gamma \neq 5/3$ by including the effects of turbulent heating of the solar wind in the inner and outer heliosphere. We are also developing a generalization of the code that will encompass a variety of solar cycle conditions.

[26] **Acknowledgments.** We acknowledge the use of Voyager 1 and 2 plasma and magnetic field data supplied by the National Space Science Data Center. This work was performed, in part, while one of the authors (AVU) held a National Research Council Senior Research Associateship at the NASA Goddard Space Flight Center. The work of AVU was also supported, in part, by grant NNG05GB46G to the University of Delaware. MLG acknowledge the support of a NASA Solar Heliospheric Supporting Research and Technology award.

[27] Shadia Rifai Habbal thanks Thomas E. Holzer and Gary P. Zank for their assistance in evaluating this paper.

References

Baranov, V. B., and Y. G. Malama (1993), Model of the solar wind interaction with the local interstellar medium: Numerical solution of self-consistent problem, *J. Geophys. Res.*, *98*(A9), 15,157–15,163.

Blum, P. W., and H. J. Fahr (1970), Interaction between interstellar hydrogen and the solar wind, *Astron. Astrophys.*, *4*, 280–290.

Burlaga, L. F., N. F. Ness, J. W. Belcher, A. Szabo, P. A. Isenberg, and M. A. Lee (1994), Pickup protons and pressure-balanced structures: Voyager 2 observations in merged interaction regions near 35 AU, *J. Geophys. Res.*, *99*(A11), 21,511–21,524.

Burlaga, L. F., N. F. Ness, J. W. Belcher, and Y. C. Whang (1996), Pickup protons and pressure-balanced structures from 39 to 43 AU: Voyager 2 observations during 1993 and 1994, *J. Geophys. Res.*, *101*(A7), 15,253–15,532.

Fahr, H. J. (1973), Non-thermal solar wind heating by supra-thermal ions, *Solar Phys.*, *30*, 193–206.

Gazis, P. R., A. Barnes, J. D. Mihalov, and A. J. Lazarus (1994), Solar wind velocity and temperature in the outer heliosphere, *J. Geophys. Res.*, *99*(A4), 6561–6573.

Holzer, T. E. (1972), Interaction of the solar wind with the neutral component of the interstellar gas, *J. Geophys. Res.*, *77*(28), 5407–5431.

Holzer, T. E., and E. Leer (1973), Solar wind heating beyond 1 AU, *Astrophys. Space Sci.*, *24*, 335–347.

Isenberg, P. A. (1986), Interaction of the solar wind with interstellar neutral hydrogen: Three-fluid model, *J. Geophys. Res.*, *91*(A9), 9965–9972.

Isenberg, P. A., C. W. Smith, and W. H. Matthaeus (2003), Turbulent heating of the distant solar wind by interstellar pickup protons, *Astrophys. J.*, *592*, 564–573.

Linde, T. J., T. I. Gombosi, P. L. Roe, K. G. Powell, and D. L. De Zeeuw (1998), Heliosphere in the magnetized local interstellar medium: Results of a three-dimensional MHD simulation, *J. Geophys. Res.*, *103*(A2), 1889–1904.

MacCormack, R. W. (1971), Numerical solution of the interaction of a shock wave with a laminar boundary layer, in *Proceedings of the Second International Conference on Numerical Methods in Fluid Dynamics*, *Lecture Notes in Phys.*, vol. 8, edited by M. Holt, pp. 151–163, Springer, New York.

Opher, M., P. C. Liewer, T. I. Gombosi, W. B. Manchester, D. L. De Zeeuw, I. V. Sokolov, and G. Tóth (2003), Probing the edge of the solar system: Formation of an unstable jet-sheet, *Astrophys. J.*, *591*, L61–L65.

Pauls, H. L., and G. P. Zank (1996), Interaction of a nonuniform solar wind with the local interstellar medium, *J. Geophys. Res.*, *101*(A8), 17,081–17,092.

Pauls, H. L., and G. P. Zank (1997), Interaction of a nonuniform solar wind with the local interstellar medium: 2. A two-fluid model, *J. Geophys. Res.*, *102*(A9), 19,779–19,787.

Pauls, H. L., G. P. Zank, and L. L. Williams (1995), Interaction of the solar wind with the local interstellar medium, *J. Geophys. Res.*, *100*(A11), 21,595–21,604.

Phillips, J. L., et al. (1995), Ulysses solar wind plasma observations at high southerly latitudes, *Science*, *268*, 1030–1033.

Pizzo, V. J. (1982), A three-dimensional model of corotating streams in the solar wind: 3. Magnetohydrodynamic flows, *J. Geophys. Res.*, *87*(A6), 4374–4394.

Richardson, J. D., and C. W. Smith (2003), The radial temperature profile of the solar wind, *Geophys. Res. Lett.*, *30*(5), 1206, doi:10.1029/2002GL016551.

Richardson, J. D., K. I. Paularena, A. J. Lazarus, and J. W. Belcher (1995), Evidence for a solar wind slowdown in the outer heliosphere?, *Geophys. Res. Lett.*, *22*(12), 1469–1472.

Semar, C. L. (1970), Effect of interstellar neutral hydrogen on the termination of the solar wind, *J. Geophys. Res.*, *75*(34), 6892–6898.

Smith, C. W., P. A. Isenberg, W. H. Matthaeus, J. D. Richardson, S. Oughton, and G. P. Zank (2004), Heating the outer heliosphere by pickup protons, in *Physics of the Outer Heliosphere*, edited by V. Florinski, N. V. Pogorelov, and G. P. Zank, *AIP Conf. Proc.*, *719*, 359–364.

Totten, T. L., J. W. Freeman, and S. Arya (1995), An empirical determination of the polytropic index for the free-streaming solar wind using Helios 1 data, *J. Geophys. Res.*, *100*(A1), 13–17.

Usmanov, A. V. (1996), A global 3-D MHD solar wind model with Alfvén waves, in *Solar Wind Eight*, edited by D. Winterhalter et al., *Aip Conf. Proc.*, *382*, 141–144.

Usmanov, A. V., and M. L. Goldstein (2003), A tilted-dipole MHD model of the solar corona and solar wind, *J. Geophys. Res.*, *108*(A9), 1354, doi:10.1029/2002JA009777.

Usmanov, A. V., M. L. Goldstein, B. P. Besser, and J. M. Fritzer (2000), A global MHD solar wind model with WKB Alfvén waves: Comparison with Ulysses data, *J. Geophys. Res.*, *105*(A6), 12,675–12,695.

Verma, M. K., D. A. Roberts, and M. L. Goldstein (1995), Turbulent heating and temperature evolution in the solar wind plasma, *J. Geophys. Res.*, *100*(A10), 19,839–19,850.

Wang, C., and J. D. Richardson (2001), Energy partition between solar wind protons and pickup ions in the distant heliosphere: A three-fluid approach, *J. Geophys. Res.*, *106*(A12), 29,401–29,407.

Wang, C., J. D. Richardson, and J. T. Gosling (2000), A numerical study of the evolution of the solar wind from Ulysses to Voyager 2, *J. Geophys. Res.*, *105*(A2), 2337–2344.

Weber, E. J., and L. Davis (1967), The angular momentum of the solar wind, *Astrophys. J.*, *148*, 217–227.

Whang, Y. C. (1998), Solar wind in the distant heliosphere, *J. Geophys. Res.*, *103*(A8), 17,419–17,428.

Whang, Y. C., L. F. Burlaga, and N. F. Ness (1996), Pickup protons in the heliosphere, *Space Sci. Rev.*, *78*, 393–398.

Whang, Y. C., L. F. Burlaga, Y.-M. Wang, and N. R. Sheeley (2003), Solar wind speed and temperature outside 10 AU and the termination shock, *Astrophys. J.*, *589*(1), 635–643.

Williams, L. L., G. P. Zank, and W. H. Matthaeus (1995), Dissipation of pickup-induced waves: A solar wind temperature increase in the outer heliosphere?, *J. Geophys. Res.*, *100*(A9), 17,059–17,067.

Zank, G. P. (1999), Interaction of the solar wind with the local interstellar medium: a theoretical perspective, *Space Sci. Rev.*, *89*, 413–688.

Zank, G. P., H. L. Pauls, L. L. Williams, and D. T. Hall (1996), Interaction of the solar wind with the local interstellar medium: A multifluid approach, *J. Geophys. Res.*, *101*(A10), 21,639–21,655.

M. L. Goldstein and A. V. Usmanov, Code 612.2, NASA Goddard Space Flight Center, Greenbelt, MD 20771, USA. (melvyn.l.goldstein@nasa.gov; arcadi.usmanov@gsfc.nasa.gov)